IEEE Access
Multidisciplinary | Rapid Review | Open Access Journal

Received March 9, 2021, accepted April 1, 2021, date of publication April 14, 2021, date of current version April 26, 2021.

Digital Object Identifier 10.1109/ACCESS.2021.3073071

Transient Test and AC Loss Study of a Cryogenic Propulsion Unit for All Electric Aircraft

FANGJING WENG, MIN ZHANG, (Member, IEEE), ABDELRAHMAN ELWAKEEL, (Graduate Student Member, IEEE), TIAN LAN, NEVILLE MCNEILL, AND WEIJIA YUAN, (Senior Member, IEEE)

Applied Superconductivity Laboratory, Department of Electronic and Electrical Engineering, University of Strathclyde, Glasgow G1 1XQ, U.K.

Corresponding author: Min Zhang (min.zhang@strath.ac.uk)

This work was supported in part by the Royal Academy of Engineering Research Fellowship under the Project title Fully Superconducting Machines for Next Generation Aircraft Propulsion, and in part by the EPSRC-Funded Project Developing Highly Efficient HTS AC Windings for Fully Superconducting Machines under Grant EP/P002277/2. The work of Fangjing Weng was supported by the Chinese Scholar Council under Grant 201908060381.

ABSTRACT This paper reports a pioneering demonstration platform of a cryogenic propulsion unit at liquid nitrogen temperature. A high temperature superconducting (HTS) machine is connected with a cryogenic power rectifier in a generator mode to prove the feasibility of a cryogenic propulsion unit for electric aircraft propulsion applications. Machine operation was carried out with a special focus on the total heat dissipation inside the HTS AC windings. Different types of 2G HTS tapes were tested to provided data for stator coils' design. The transient operation was carried out to represent a short-circuit failure in one of the power electronic devices. The test shows AC loss performance of the HTS windings using calorimetric method during the short circuit event, indicating the importance of developing protection schemes for the cryogenic propulsion units to prevent damage to the HTS components. The paper provides initial insights into the interaction between superconducting machines and cryogenic power electronics within a cryogenic propulsion unit. It is an important first step to understand and further develop cryogenic propulsion technology for future electric aircraft.

INDEX TERMS 2G HTS machine, cryogenic power electronic, AC loss, calorimetric method.

I. INTRODUCTION

To address the environmental impacts of air transportation and achieve long-term sustainability, the aviation industry has called for next generation aircraft with reduced emissions [1]–[10]. One underpinning technology is the conversion from the direct use of fossil fuels to electric drives. Electric propulsion enables the full synergistic benefits of the coupling between airframe aerodynamics and the propulsion thrust stream by distributing thrust over the airframe, resulting in a dramatic reduction of aircraft-related fuel burn, emissions, and noises. This technology has been demonstrated by the Airbus E-Fan project [11], which is the first prototype electric aircraft using on-board lithium batteries to power electric motors. Also, NASA's Advanced Air-Transport Technology Project has proposed goals for the next generation of aircraft for commercial aviation in areas of reducing fuel burn and emissions. The goals are challenging and require the new structure of motors, generators, cables and power electronic devices to increase the power density significantly [12].

To be specific, one of the major technical challenges for expanding electric aircraft to large fleets and over long-haul distances is the low power density of electrical machines [3], [9], [13]. In other words, conventional electrical motors are too heavy to drive aircraft over long flight distances (>1 hours). To provide the multi-megawatt levels of power necessary to drive large electric aircraft while keeping them light and compact, new technologies must be developed to increase the power density of electric motors. High temperature superconductors (HTS) offer a transformative way to increase machine power densities, because their current-carrying capability is more than twenty times that of copper. The operational temperatures of HTS (25 - 77 K) are much higher than low temperature superconductors (4.2 K), resulting in greatly reduced cooling costs for large scale applications. Fully HTS machines, which use HTS in both the direct current (DC) and alternating current (AC) windings to increase the electrical loading and magnetic loading, can

The associate editor coordinating the review of this manuscript and approving it for publication was Lei Chen.

This work is licensed under a Creative Commons Attribution 4.0 License. For more information, see https://creativecommons.org/licenses/by/4.0/

increase the power density of electrical machines by up to 400% [14], [15]. Therefore, they are the key technology to enable aviation electrical propulsion [5].

Assuming that fully HTS machines can meet power density requirement, a cryogenic power network is still required to transfer the propulsion electricity. HTS generators, HTS motors, HTS cables are required to operate at cryogenic temperature. Considering the efficiency of the cryogenic-refrigerator, a closed loop cooling system would be used to ensure reliability and increase the efficiency of the cryogenic cooling systems [8], [16], [17]. This means power electronic devices would also run in cryogenic operating temperature (25 - 77 K). In this propulsion system, cryogenic temperature would improve the heat dissipation of these power electronic devices, and significantly increase the power density and enhance the reliability [18], [19].

More recently, NASA is exploring the potential of liquid hydrogen fuel cells combined with cryogenic propulsion technology to achieve all-electric airliners with no greenhouse gas emissions. Airbus and Rolls-Royce also investigated a superconducting network for hybrid propulsion purpose by understanding how the various components affect the overall system performance in terms of positive fuel save. Currently, key network components including superconducting machines, superconducting cables and cryogenic power electronics have been studied [4], [5], [17], [20], [21]. Operating power electronic devices at cryogenic temperatures can reduce the temperature gradient experienced in the network and minimise the cooling requirement for all systems. However, the feasibility of operating power electronic devices at cryogenic temperatures in conjunction with superconducting machines has not been proved, although individual device tests have been done at cryogenic temperatures [19].

The aim of this paper is to demonstrate, for the first time, the testing of a cryogenic propulsion unit consisting of an HTS machine and a cryogenic power rectifier. The interaction between the machine and the rectifier are studied in transient modes. The transient study focuses on understanding how a power electronic device failure can potentially damage the HTS machine.

The paper is organised into four sections. The second section introduces a novel HTS demonstrating machine which allows the measurement of HTS armature coil AC losses. This section also tested two 2G HTS coil in order to provide data for machine design. The third section analyses the transient test results, which led to the quench of the HTS armatures. The first-of-its-kind results demonstrated in this paper show the feasibility of a cryogenic propulsion unit. It also reveals the importance to develop protection functions for such a novel unit. The final section is the summary and conclusion.

II. A NOVEL CRYOGENIC PROPULSION TESTING PLATFORM

The whole platform for a cryogenic propulsion unit has been developed at the Applied Superconductivity Laboratory of the University of Strathclyde [22]. In this setup, the total AC loss can be measured by calorimetric method [23]–[29]. Fig. 1. shows the platform, which consists of a conventional DC motor, an axial-flux HTS machine in generator mode, a cryogenic power electronic testing chamber and a control /data acquisition system. Consequently, the DC machine drives the HTS machine as a generator. The three-phase output from the HTS machine is connected to a cryogenic power rectifier, feeding DC electricity into power resistances, as shown in Fig. 1.

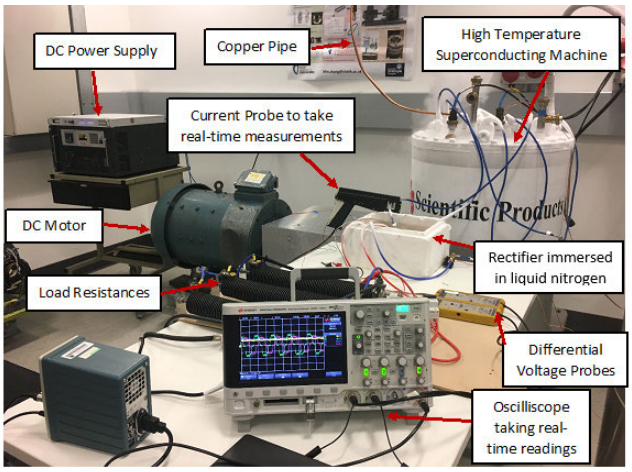

FIGURE 1. Cryogenic propulsion unit test platform.

A. THE HTS MACHINE WITH AC LOSS MEASUREMENT

In electrical machines, the HTS AC windings are subjected to a combined rotational magnetic field and AC current. The AC loss depends not only on the magnitudes of the magnetic field and transport current, but also on the phase shift between the field and the current. Different magnetic field directions and different phase shifts give different levels of AC loss. The AC loss studies in HTS tapes and coils have been carried out throughout the duration of the development of HTS devices [21], [26], [30]–[37]. There are two established methods for measuring AC loss. The transport loss and magnetization loss of HTS can be measured by the electrical method. The total AC loss, which includes both transport loss and magnetization loss, can only be measured by the calorimetric method [21]. Previous studies have measured the total AC loss of HTS coils using both the liquid nitrogen boil-off method and the temperature rising method [24], [25], [38]. However, the rotational magnetic field, which is an important feature of electrical machines, has not previously been studied in AC loss experiments.

To understand the impact of rotational magnetic fields on the HTS armature losses and the whole machine efficiency, an axial-flux HTS machine platform has been designed and developed to measure the AC loss of an HTS stator in a rotational magnetic field. The HTS machine consists of a 2-pole-pair of permanent magnet rotor discs to generate a peak 0.45 T

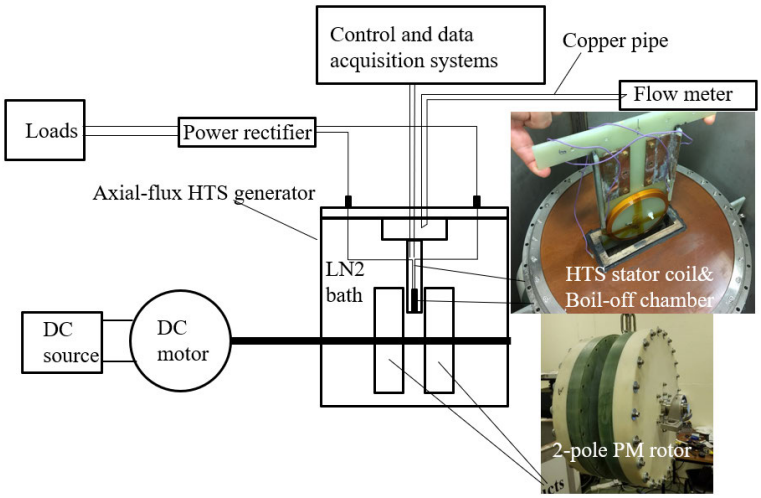

FIGURE 2. Structure of the HTS generator.

in a 50-mm air-gap, and an air-cored three-phase HTS stator plate. The stator disc is located between the two rotor discs. The stator is equipped with two HTS coils in Phase A and four copper coils in Phases B and C. Also, as Fig. 2 shows, the whole machine is hosted in a vacuum-walled cryostat filled with liquid nitrogen (LN_2) during operation and the top HTS coil was placed in a measurement chamber to measure the AC loss by the calorimetric method, the measurement chamber is fully immersed in LN_2 inside the machine cryostat to minimise heat exchange. Previous study had carefully calibrated and validated this system [22], to provide AC losses of stator coil when the machine was real-time operating.

The AC loss of the HTS coil is measured by the amount of liquid nitrogen being evaporated as nitrogen gas using a gas flow meter. Fig. 2 shows a copper pipe that connects to the flow meter. Theoretically, the latent heat for liquid nitrogen is 160.6 J/mL, which means every 0.257 standard litre nitrogen gas per minute for every Watt of power (SLPM/W). Therefore, by measuring the nitrogen gas boil-off flow rate, the total AC losses in the measurement chamber can be quantified by a set of calibration procedures, to minimize the errors caused by current leads, environment heat radiation, rotor and stator [22]. Total AC loss of period T can be calculated by (1) [34].

$$Q = \int_T \frac{F(t)}{K} dt. \tag{1}$$

where Q (Joule) is the total heat produced by measured HTS coil for a duration of T, F_t is the flow rate of nitrogen gas boiled off in the measurement chamber after calibration. $K = 0.256$ (SLPM/W) is the flow rate constant in our setup.

This system provides a synchronous generator to generate 3 phase voltages, the measured HTS coil in HTS phase can provide the AC losses data while running the machine, 2 copper phases were impedance match between phase A to provide the same voltage amplitude, in FFT analysis only 3rd harmonic exist in the stator, and the phases are star-connected to remove the 3rd harmonic. The rated line-to-line voltage is 40 V. The Coil #1 is made of 25 meters of 2G YBCO HTS coated conductor, with a critical current measured as 53 A in a 0.45 T magnetic field. The peak phase current must be lower than 53 A to prevent HTS coil quench. Due to the critical current of the HTS coil, the rated current is set as 40 A. The generator was connected with a power rectifier also run in LN_2 temperature, then connected with adjustable power resistors, as Fig. 2 shown. The data acquisition systems can record the temperature, phase voltage, phase current, nitrogen gas flow rate to calculate total AC losses.

Several industrial manufacturers are able to provided REBCO coated conductors for multiple purposes, due to the differences between REBCO materials, the $Jc(B)$ characteristics of the various tapes could be different. For 2G HTS tapes, the critical current is decreased when external magnetic field increase, thus, based on critical-state model, the change in AC current and external AC magnetic field cause the magnetic field redistribution inside the HTS tapes. The transport AC loss is caused by AC current, and the total loss is caused by AC current as well as AC magnetic field. As a result, in machine environment, good $Jc(B)$ characteristics of the tape can enhance the AC loss performance.

Thus, another Coil #2 is prepared to make a comparison. Coil #2 is made of 15.5 meters of 2G GdBCO HTS tape. The YBCO tape is from Superpower SCS4050 including 1 μm YBCO, the GdBCO tape is from Sunam SAN04150 including 1 - 3 μm GdBCO, the total wire thickness of both wires is 100 - 110 μm. The single tape's critical current for Coil #1 and Coil #2 is 143 A and 150 A respectively. Fig. 3 shows the picture of two coils. The parameters of two coils are shown in Table 1.

The critical current results are shown in Fig. 4. The red curve shows the critical current of Coil #1, and blue curve demonstrates the critical current of Coil #2. The curves with

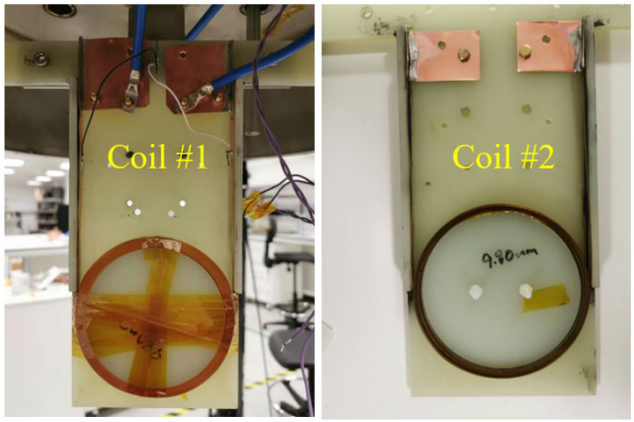

FIGURE 3. Coil #1 and Coil #2.

TABLE 1. Description of manufactured double pancake coil.

	Coil #1	Coil #2
HTS type	Superpower SCS4050	Sunam SAN04150
Coil Length	25 m	15.5 m
Coil inner/outer diameter	95 mm/102.8 mm	98 mm/103.0 mm
Turns per layer	39	25
Total coil turns	78	50
Self-field Ic	72 A	102 A
In-field Ic (0.45 T)	53 A	59 A
Insulation	Kapton tape	Kapton tape

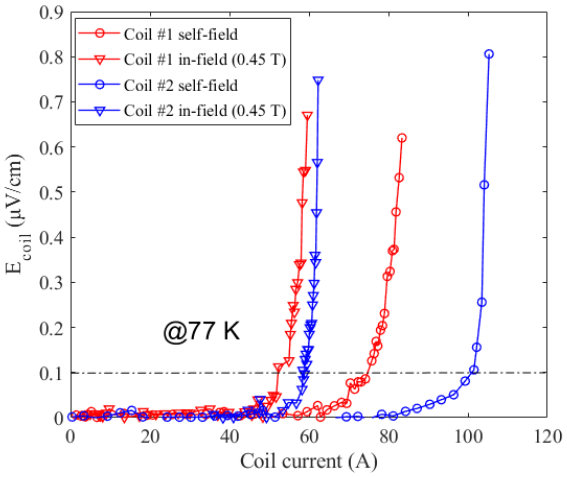

FIGURE 4. Critical currents of Coil #1 and Coil #2.

triangle signs indicated the result in 0.45 T magnetic field, the centre of the coil coincides with the centre of the permanent magnet of the rotor, the curves with circle signs indicated the critical results with self-field. Fig. 4 indicated that the critical current drop from self-field to in-field. By using 0.1 μV/cm criteria, for Coil #1, the critical current reduces from 72 A to 53 A when a 0.45 T magnetic field apply, which means a 26.4% drop. For Coil #2, the critical current reduces from 102 A to 59 A, which means a 42.2% drop. Although Coil #2 has higher critical current in 77 K, the critical current decreased rapidly with increasing magnetic field. Thus, Coil #1 has a better $Jc(B)$ characteristic.

In order to evaluate the difference between the two coils, the experimental value of transport loss is measured by the

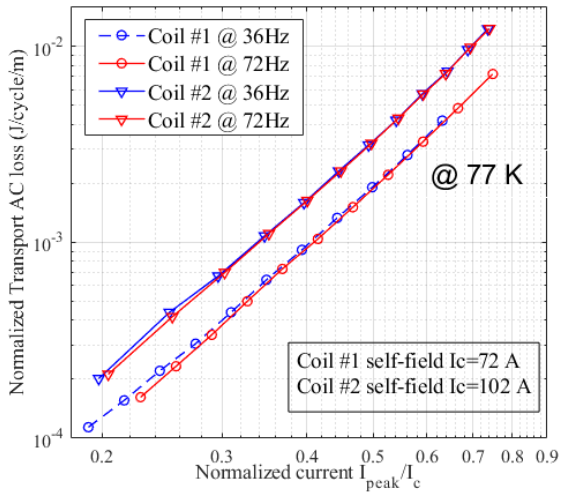

FIGURE 5. Transport loss in self-field of Coil #1 and Coil #2.

electrical method [32], [34]. The loss voltage can be compensated by a cancelling coil, as shown in (2), where i and u_c are the transport current and voltage after compensation by cancelling coil. T refers to the cycle of AC current. Two frequencies were chosen for this experiment. The normalized transport loss versus normalized transport current measured by the electrical method is shown in Fig. 5, according to our AC power supply's limit, the frequencies are chosen at 36 Hz and 72 Hz, and the results are shown by normalized AC loss (Joule/cycle/m), our results indicate that the normalized transport AC loss of both coils are frequency independent. According to the normalized transport AC loss results, the transport loss of Coil #1 is 43.1% lower than Coil #2.

$$Q = \int_T (i \cdot u_c)\, dt \tag{2}$$

The total AC loss versus normalized current were measured by calorimetric method are shown in Fig. 6. The maximum rotational speed is 300 RPM due to the limitation of the bearing in 77 K, which means a 10 Hz output. Thus, the frequencies are set at 5 Hz and 10 Hz, the transport currents are chosen from 10 A to 50 A, in our machine, the rotor generate a peak 0.45 T rotational magnetic field. According to the normalized total AC loss results, the normalized total AC loss of both coils are frequency independent, and the total loss of Coil #1 is 65.8% lower than Coil #2. Also, Fig. 4 and Fig. 5 indicate that the Coil #1 has lower transport AC loss and fewer in-field critical current reduction. As a result, two coils have the same outer diameter, Coil #1 has more length of tapes and more turns, but AC losses are significantly lower than Coil #2, considering the operating reliability for the next stage machine experiments, the Coil #1 is finally chosen for next stage tests.

B. CRYOGENIC POWER RECTIFIER

A full-bridge three-phase rectifier was developed and tested in LN_2. The diode chosen is a Silicon fast recovery type made

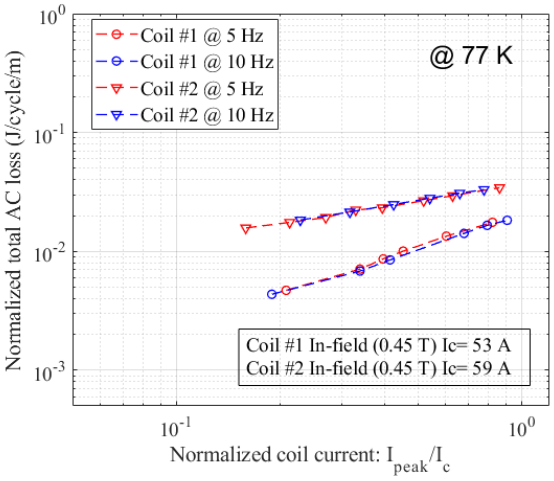

FIGURE 6. Total loss of Coil #1 and Coil #2 in a 0.45 T rotational magnetic field.

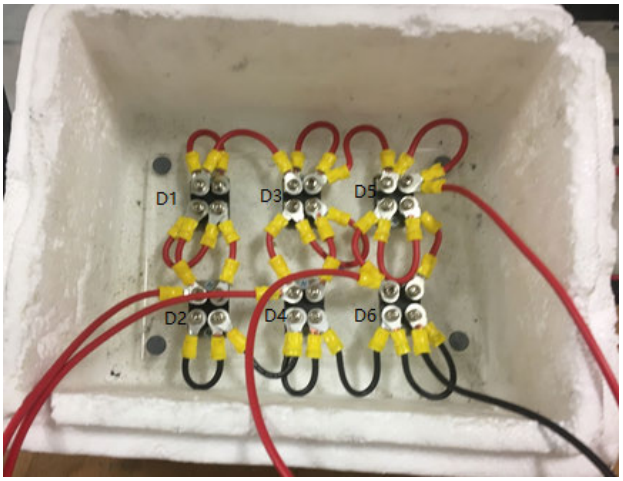

FIGURE 7. Rectifier of 6 diodes.

by Microsemi® (type APT 2 × 101 DQ120J). Different types of diode including Silicon, Silicon Carbide Schottky and Fast Recovery Epitaxial Diodes have been tested at cryogenic and room temperature. However, this particular diode has been chosen as it offers low power dissipation at cryogenic temperatures. The forward voltage of the diode was measured at 25 A at both room temperature and 77 K and there was found to be a significant reduction, from 1.6 V at room temperature to 1.3 V at 77 K. This would result in a reduction of the power losses of the rectifier at cryogenic temperatures.

C. SYSTEM OPERATION CIRCUIT

Fig. 8 shows the system circuit. The system operates in a generator mode, with a three-phase output from the HTS machine (Phase *A* is superconducting). During steady-state operation, the HTS machine is connected to the three-phase rectifier which is cooled down by liquid nitrogen. The rectifier is connected with a LC filter circuit to a resistive load bank. To study transient operation, a short-circuit was introduced

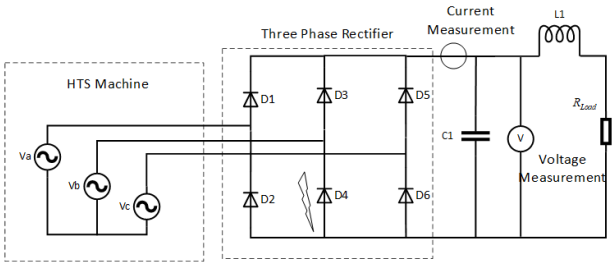

FIGURE 8. Circuit diagram of the cryogenic propulsion unit.

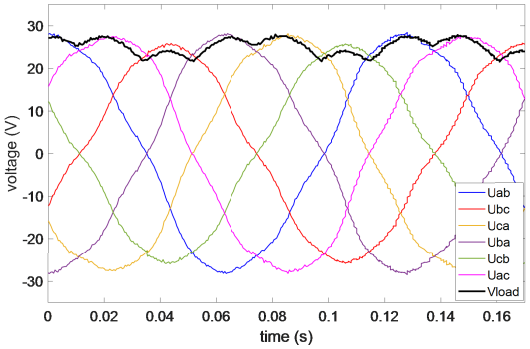

FIGURE 9. No-load output three-phase armature voltage and the load voltage at 240 RPM.

across *D*4. A low pass filter, consisting of an inductor *L*1 and a capacitor *C*1 as shown in Fig. 7 has been added to reduce the oscillations in the output current and voltage. The inductance has been chosen at 40 μH and the capacitance at 1 μF due to the relatively low operating speed of the system. The parameters measured during the tests include the total nitrogen gas boil-off rate (the total AC loss) in an HTS coil in Phase *A*, the three-phase voltage/current, the load current, and the rotational speed of the system.

III. TRANSIENT ANALYSIS OF THE PROPULSION UNIT

The system was operated at 240 RPM in generator mode. Before commencing rotation, the HTS machine and the rectifier were fully cooled down to 77 K by LN_2. The speed control of the rotational shaft was implemented via the separately excited DC motor by adjusting the DC power supply input. Fig. 9 shows the measured operating voltages and the load voltage. The imbalance in the voltage outputs is due to the geometry difference between Phase A (HTS tape windings) and Phases *B* and *C* (copper wire windings).

A sudden short-circuit in a cryogenic propulsion network can serious impact superconducting machines and the whole aircraft electrical system. It can potentially happen when there is a device or insulation failure in the cryogenic environment, leading to permanent damage of HTS windings and consequently affecting the performance of the whole system. In this section, the effect of a short circuit event at the power electronic side of the propulsion unit, which can be caused

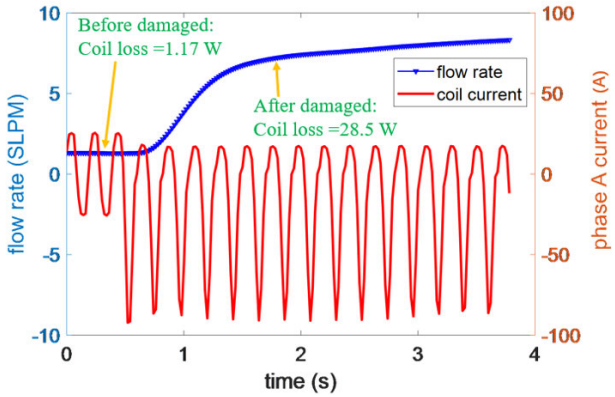

FIGURE 10. Phase *A* current during the short-circuit event and the corresponding nitrogen gas boil-off rate measured by the flow meter.

TABLE 2. Parameters used in system simulation.

R_{load}	Measured resistance for the load resistance bank	0.33 Ω
$R_{HTScoil}$	Measured resistance for the HTS coil joints	2 μΩ
R_{quench}	Equivalent resistance after the HTS coil quenches	60 μΩ
$R_{coppercoil}$	Measured resistance for copper coils	98 μΩ

by the failure of a diode, is studied both experimentally and numerically.

As shown in Fig. 8, a short-circuit was introduced across *D*4 at approximately 0.5 s. When the short-circuit event occurs, there was a loud sound from the machine, indicating a quench event. The nitrogen gas boil-off rate increases dramatically, as shown in Fig. 10, which indicated the coil loss increase from 1.01 W to 28.5 W. The HTS coil was inspected physically and electrically afterwards. There was no obvious burning sign of the coil due to the quench induced by the short-circuit. But the outermost layers of the coil has been deformed slightly due to unbalanced Lorentz forces during the short-circuit, as shown in Fig. 11. The critical current of the measured HTS coil remains the same, but the AC loss values are 28 times higher than before the short-circuit event. This indicates that weak points had been introduced into the coil, caused by the unbalanced Lorentz forces or the large amount of heat generated during the quench.

Fig. 12 shows the phase-phase output voltages and the load voltage before and immediately after the short-circuit event. The sample rate is 50 samples/s due to DAQ system limitation. During the experiment, diode *D*4 was short-circuited as seen in Fig. 8, meaning that when V_b is larger than V_a or V_c, there is a short-circuit across line voltage V_{ba} and V_{bc}, which in return would cause very large current passing through the phases, and eventually causing the superconducting coil in Phase *A* to quench.

To better understand what happened during the short-circuit event, we performed a MATLAB simulation based on Fig. 13. The parameters that were measured directly from the system are listed in Table 2. The simulation simplifies the quench progress of HTS windings by ignoring the quench propagation process, and uses two resistance values to represent the HTS winding before and after the quench respectively. The results shows good agreements between experiment and simulation have been found as shown in Fig. 14 and Fig. 15.

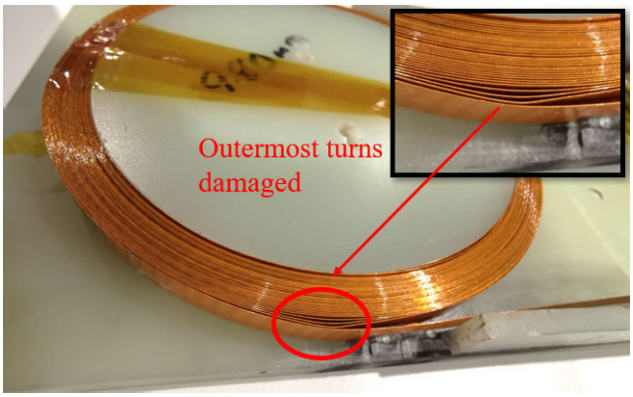

FIGURE 11. Damaged coil after quench.

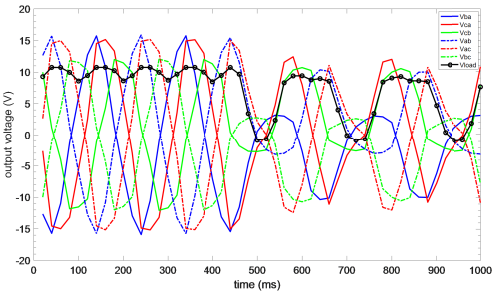

FIGURE 12. Measured voltages during the short-circuit event.

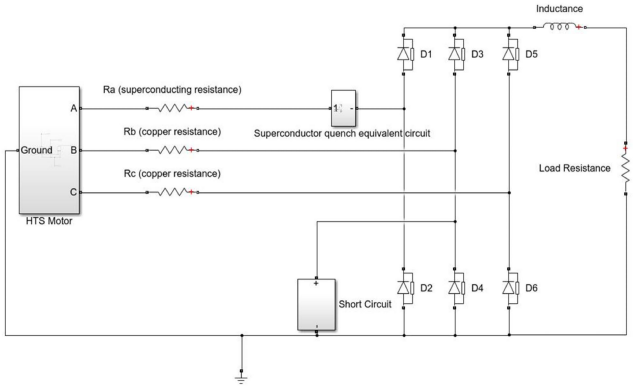

FIGURE 13. Simulation model.

Fig. 14 shows a comparison between the experimental and simulation results for the output voltages. When the short-circuit happens, the negative half cycles of V_{ab} are around −3 V, corresponding to voltage drops from *D*2 and the copper cables when an over-current flowed from phase *B* to phase *A*. Similarly, the positive half cycles of V_{bc} are around 3 V, corresponding to voltage drops from *D*6 and the copper cables when an over-current flowed from phase *B* to phase *C*. V_{ca} is largely unaffected. The slight drop in voltage is the

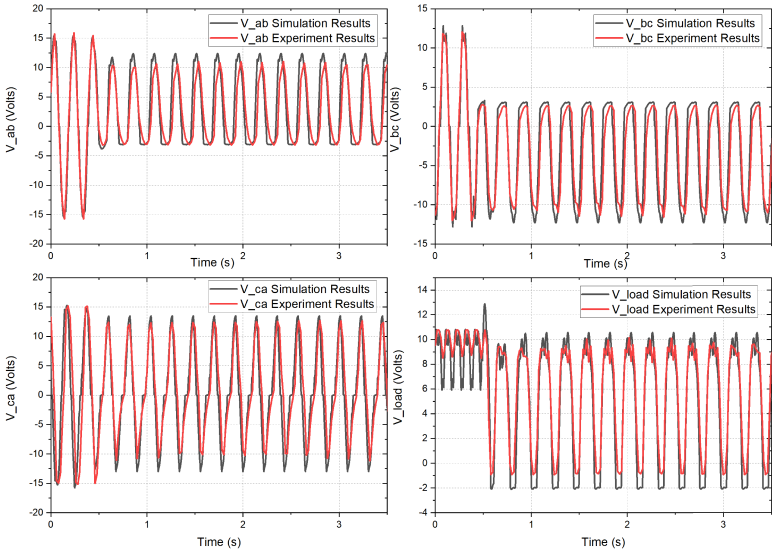

FIGURE 14. Measured voltages during the short-circuit event.

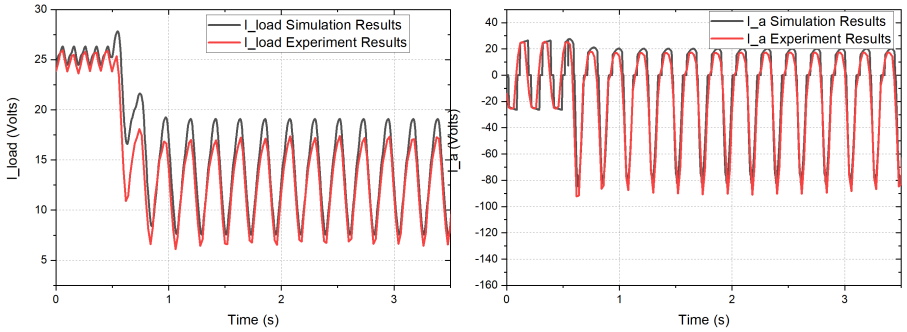

FIGURE 15. Comparison between experiment and simulation for the load current Iload and the phase *A* current *Ia*.

result of slowing-down of the DC machine from 150 RPM to 136.5 RPM. This results in the peak induced EMF being reduced from 15 V to 12 V. A similar voltage drop is also observed in the positive half cycles of V_{ab} and the negative half cycles of V_{bc}.

Fig. 15. shows the comparison between experimental results and simulation for the measured load current and Phase *A* current. During the pre-fault period, the load current had small oscillations around 25 A. After the fault, the load current has been significantly reduced as seen in Fig. 12. The peak Phase *A* current is approximately -80 A to -90 A for the negative half cycles. This is much higher than the critical current of the HTS coil, which is 53 A under the rotational field conditions. Consequently, the HTS coil quenches, leading to the large nitrogen boil-off rate as shown in Fig. 10. The Phase *A* current is asymmetric, because the short-circuit only happens when V_b is higher than V_a and V_c. For positive half cycles, the slight reduction in the Phase *A* current is the result of EMF reduction.

IV. FUTURE WORK AND CONCLUSION

We have developed a testing platform for cryogenic propulsion applications. This paper reports the test on the cryogenic propulsion unit in both steady/transient conditions. The advantage of the platform is that the total AC loss of the HTS armature can be measured whilst connected to different types of power electronics to study the system impact on the HTS machine efficiency. More importantly, how the HTS machine reacts in a transient condition from the network point of view can also be tested. The transient operation confirms that the HTS machine windings are subjected to damage when there is a short-circuit event in the propulsion network. Fast response protection schemes for HTS machines will need to be investigated.

ACKNOWLEDGMENT

The authors would like to thank the Academy for their technical support.

REFERENCES

[1] M. J. Armstrong, C. A. H. Ross, M. J. Blackwelder, and K. Rajashekara, "Propulsion system component considerations for NASA N3-X turbo-electric distributed propulsion system," *SAE Int. J. Aerosp.*, vol. 5, no. 2, pp. 344–353, Oct. 2012.

[2] M. K. Bradley and C. K. Droney, *Subsonic Ultra Green Aircraft Research: Phase 2. Hybrid Electric Design Exploration*, vol. 2. Hampton, VA, USA: NASA, 2015. [Online]. Available: https://ntrs.nasa.gov/citations/20150017039

[3] A. S. Gohardani, G. Doulgeris, and R. Singh, "Challenges of future aircraft propulsion: A review of distributed propulsion technology and its potential application for the all electric commercial aircraft," *Prog. Aerosp. Sci.*, vol. 47, no. 5, pp. 369–391, Jul. 2011.

[4] C. A. Luongo, P. J. Masson, T. Nam, D. Mavris, H. D. Kim, G. V. Brown, M. Waters, and D. Hall, "Next generation more-electric aircraft: A potential application for HTS superconductors," *IEEE Trans. Appl. Supercond.*, vol. 19, no. 3, pp. 1055–1068, Jun. 2009.

[5] P. J. Masson and C. A. Luongo, "HTS machines for applications in all-electric aircraft," in *Proc. IEEE Power Eng. Soc. Gen. Meeting*, Jun. 2007, pp. 1–6.

[6] P. J. Masson and C. A. Luongo, "High power density superconducting motor for all-electric aircraft propulsion," *IEEE Trans. Appiled Supercond.*, vol. 15, no. 2, pp. 2226–2229, Jun. 2005.

[7] B. Sarlioglu and C. T. Morris, "More electric aircraft: Review, challenges, and opportunities for commercial transport aircraft," *IEEE Trans. Transp. Electrific.*, vol. 1, no. 1, pp. 54–64, Jun. 2015.

[8] F. Berg, J. Palmer, P. Miller, M. Husband, and G. Dodds, "HTS electrical system for a distributed propulsion aircraft," *IEEE Trans. Appl. Supercond.*, vol. 25, no. 3, pp. 1–5, Jun. 2015.

[9] G. Brown, "Weights and efficiencies of electric components of a turboelectric aircraft propulsion system," in *Proc. 49th AIAA Aerosp. Sci. Meeting Including New Horizons Forum Aerosp. Expo.*, Jan. 2011, p. 225.

[10] A.-R. Kim, K.-M. Kim, H. Park, G.-H. Kim, T.-J. Park, M. Park, S. Kim, S. Lee, H. Ha, S. Yoon, and H. Lee, "Performance analysis of a 10-kW superconducting synchronous generator," *IEEE Trans. Appl. Supercond.*, vol. 25, no. 3, pp. 1–4, Jun. 2015.

[11] L. Juvé, J. Fosse, E. Joubert, and N. Fouquet, "Airbus group electrical aircraft program, the E-Fan project," in *Proc. 52nd AIAA/SAE/ASEE Joint Propuls. Conf.*, Jul. 2016, p. 4613.

[12] N. Madavan, J. Heidmann, C. Bowman, P. Kascak, A. Jankovsky, and R. Jansen, "A NASA perspective on electric propulsion technologies for commercial aviation," in *Proc. Workshop Technol. Roadmap Large Electr. Mach.*, Urbana-Champaign, IL, USA, 2016, pp. 5–6.

[13] G. V. Brown, "Efficient flight-weight electric systems," NASA, Cleveland, OH, USA, Tech. Rep. E-661272, 2012. [Online]. Available: https://ntrs.nasa.gov/citations/20150010194

[14] K. S. Haran, S. Kalsi, T. Arndt, H. Karmaker, R. Badcock, B. Buckley, T. Haugan, M. Izumi, D. Loder, J. W. Bray P. Masson, and E. W. Stautner, "High power density superconducting rotating machines—Development status and technology roadmap," *Superconductor Sci. Technol.*, vol. 30, no. 12, 2017, Art. no. 123002.

[15] H. Karmaker, D. Sarandria, M. T. Ho, J. Feng, D. Kulkarni, and G. Rupertus, "High-power dense electric propulsion motor," *IEEE Trans. Ind. Appl.*, vol. 51, no. 2, pp. 1341–1347, Mar. 2015.

[16] J. Miller, D. Santosusso, M. Uva, K. Woods, and B. Fitzpatrick, "Naval superconducting integrated power system (SIPS)," in *Proc. 10th Intell. Ship Symp.*, Philadelphia, PA, USA, 2013, pp. 22–23.

[17] L. Graber, M. Saeedifard, M. J. Mauger, Q. Yang, C. Park, T. Niebur, S. V. Pamidi, and S. Steinhoff, "Cryogenic power electronics at megawatt-scale using a new type of press-pack IGBT," in *Proc. IOP Conf., Mater. Sci. Eng.*, 2017, vol. 279, no. 1, Art. no. 012011.

[18] K. Rajashekara and B. Akin, "A review of cryogenic power electronics–status and applications," in *Proc. Int. Electr. Mach. Drives Conf.*, May 2013, pp. 899–904.

[19] P. Haldar, H. Ye, H. Efstathiadis, J. Raynolds, M. J. Hennessy, O. M. Mueller, and E. K. Mueller, "Improving performance of cryogenic power electronics," *IEEE Trans. Appiled Supercond.*, vol. 15, no. 2, pp. 2370–2375, Jun. 2005.

[20] S. Venuturumilli, F. Berg, L. Prisse, M. Zhang, and W. Yuan, "DC line to line short-circuit fault management in a turbo-electric aircraft propulsion system using superconducting devices," *IEEE Trans. Appl. Supercond.*, vol. 29, no. 5, pp. 1–6, Aug. 2019.

[21] M. Zhang, F. Eastham, and W. Yuan, "Design and modeling of 2G HTS armature winding for electric aircraft propulsion applications," *IEEE Trans. Appl. Supercond.*, vol. 26, no. 3, pp. 1–5, Apr. 2016.

[22] F. Weng, M. Zhang, T. Lan, Y. Wang, and W. Yuan, "Fully superconducting machine for electric aircraft propulsion: Study of AC loss for HTS stator," *Superconductor Sci. Technol.*, vol. 33, no. 10, Oct. 2020, Art. no. 104002.

[23] S. P. Ashworth and M. Suenaga, "The calorimetric measurement of losses in HTS tapes due to AC magnetic fields and transport currents," *Phys. C: Supercond.*, vol. 315, nos. 1–2, pp. 79–84, Apr. 1999.

[24] J. Eikelboom, "Apparatus for calorimetric measurement of a.c. losses in superconductors," *Cryogenics*, vol. 31, no. 5, pp. 363–365, 1991.

[25] P. K. Ghoshal, T. A. Coombs, and A. M. Campbell, "Calorimetric method of AC loss measurement in a rotating magnetic field," *Rev. Sci. Instrum.*, vol. 81, no. 7, Jul. 2010, Art. no. 074702.

[26] T. Hardono, C. D. Cook, and J. X. Jin, "Measurements of AC losses in HTSC wires exposed to an alternating field using calorimetric methods," *IEEE Trans. Appl. Supercond.*, vol. 9, no. 2, pp. 813–816, Jun. 1999.

[27] N. Magnusson, S. Hörnfeldt, J. Rabbers, B. ten Haken, and H. H. ten Kate, "Comparison between calorimetric and electromagnetic total ac loss measurement results on a BSCCO/Ag tape," *Superconductor Sci. Technol.*, vol. 13, no. 3, p. 291, 2000.

[28] N. Magnusson, N. Schönborg, A. Wolfbrandt, and S. Hörnfeldt, "Improved experimental set-up for calorimetric AC loss measurements on HTSs carrying transport currents in applied magnetic fields at variable temperatures," *Phys. C: Supercond.*, vol. 354, nos. 1–4, pp. 197–201, May 2001.

[29] M. Zhang, W. Wang, Z. Huang, M. Baghdadi, W. Yuan, J. Kvitkovic, S. Pamidi, and T. A. Coombs, "AC loss measurements for 2G HTS racetrack coils with heat-shrink tube insulation," *IEEE Trans. Appl. Supercond.*, vol. 24, no. 3, pp. 1–4, Jun. 2014.

[30] M. Zhang, W. Yuan, J. Kvitkovic, and S. Pamidi, "Total AC loss study of 2G HTS coils for fully HTS machine applications," *Superconductor Sci. Technol.*, vol. 28, no. 11, Nov. 2015, Art. no. 115011.

[31] F. Gömöry, M. Vojenčiak, E. Pardo, M. Solovyov, and J. Šouc, "AC losses in coated conductors," *Superconductor Sci. Technol.*, vol. 23, no. 3, Mar. 2010, Art. no. 034012.

[32] F. Grilli and S. P. Ashworth, "Measuring transport AC losses in YBCO-coated conductor coils," *Superconductor Sci. Technol.*, vol. 20, no. 8, p. 794, 2007.

[33] Z. Hong, W. Yuan, M. Ainslie, Y. Yan, R. Pei, and T. Coombs, "AC losses of superconducting racetrack coil in various magnetic conditions," *IEEE Trans. Appl. Supercond.*, vol. 21, no. 3, pp. 2466–2469, Jun. 2011.

[34] J.-H. Kim, C. H. Kim, G. Iyyani, J. Kvitkovic, and S. Pamidi, "Transport AC loss measurements in superconducting coils," *IEEE Trans. Appl. Supercond.*, vol. 21, no. 3, pp. 3269–3272, Jun. 2011.

[35] J. Šouc, F. Gömöry, and M. Vojenčiak, "Calibration free method for measurement of the AC magnetization loss," *Superconductor Sci. Technol.*, vol. 18, no. 5, p. 592, 2005.

[36] J. Šouc, E. Pardo, M. Vojenčiak, and F. Gömöry, "Theoretical and experimental study of AC loss in high temperature superconductor single pancake coils," *Superconductor Sci. Technol.*, vol. 22, no. 1, Jan. 2009, Art. no. 015006.

[37] M. Zhang, M. Chudy, W. Wang, Y. Chen, Z. Huang, Z. Zhong, W. Yuan, J. Kvitkovic, S. V. Pamidi, and T. A. Coombs, "AC loss estimation of HTS armature windings for electric machines," *IEEE Trans. Appl. Supercond.*, vol. 23, no. 3, Jun. 2013, Art. no. 5900604.

[38] F. Grilli, E. Pardo, A. Stenvall, D. N. Nguyen, W. Yuan, and F. Gomory, "Computation of losses in HTS under the action of varying magnetic fields and currents," *IEEE Trans. Appl. Supercond.*, vol. 24, no. 1, pp. 78–110, Feb. 2014.

FANGJING WENG received the bachelor's degree in electrical engineering and automation from Tsinghua University, Beijing, China, in 2014, and the M.Sc. degree in electrical power systems with advanced research from the University of Birmingham, U.K., in 2017. He is currently pursuing the Ph.D. degree in electronic and electrical engineering with the University of Strathclyde, Glasgow, U.K. His current work focuses on 2G high temperature superconducting machine for future electric aircraft, including model design of an ac loss measurement platform, built and tested of an axial-flux superconducting machine.

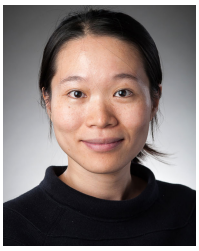

MIN ZHANG (Member, IEEE) received the bachelor's and master's degrees in electrical engineering from Tsinghua University, and the Ph.D. degree in engineering from the University of Cambridge. She spent a year as a Junior Research Fellow with the Newnham College, Cambridge. She joined the University of Bath, as a Lecturer. She joined the University of Strathclyde, as a Reader, in 2018. She is currently a Research Fellow of the Royal Academy of Engineering. Her research focuses on the application of high temperature superconductors in power system transmission, renewable generation, and electric transportation.

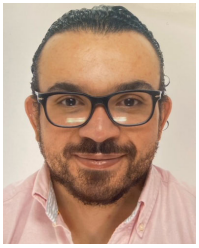

ABDELRAHMAN ELWAKEEL (Graduate Student Member, IEEE) received the B.Sc. and M.Sc. degrees from Alexandria University, Egypt. He is currently pursuing the Ph.D. degree in electronic and electrical engineering with the University of Strathclyde, Glasgow, U.K. He has worked with ABB for a period of two years. His research interests include cryogenic power electronics and transportation electrification.

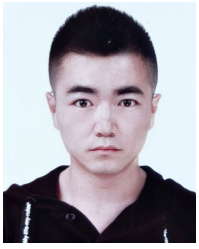

TIAN LAN was born in Meishan, Sichuan, China, in 1992. He received the Bachelor of Science (B.Sc.) degree in thermal energy and power engineering from North China Electric Power University (NCEPU), Baoding, China, in 2014, and the Master of Engineering (M.Eng.) degree in electrical engineering from Texas A&M University, in 2016. He is currently pursuing the Doctor of Philosophy (Ph.D.) degree in applied superconductivity with the Faculty of Electronic and Electrical Engineering, University of Strathclyde. His research interests include studying ways to minimize AC loss of 2G HTS coils for future fully superconducting machines. He has collaborated actively with researchers in several other disciplines of electronic and electrical engineering.

NEVILLE MCNEILL received the Ph.D. degree in power electronics from Napier University, Edinburgh, U.K., in 2008. He was with electric vehicle and renewable energy companies. From 2004 to 2016, he was with the University of Bristol, Bristol, U.K., where he was a latterly Senior Lecturer in power electronics. Since 2016, he has been a Senior Research Fellow in power electronics with the Power Electronics, Drives and Energy Conversion Group, Department of Electronic and Electrical Engineering, University of Strathclyde, Glasgow, U.K. His main research interests include the application of wide-band gap and silicon devices to realize high-efficiency multi-kilowatt power electronic conversion for aerospace, renewable energy, and electric vehicle applications. He is a member of the Institution of Engineering and Technology, a Chartered Engineer with the Engineering Council of the U.K., and a Fellow of the Higher Education Academy.

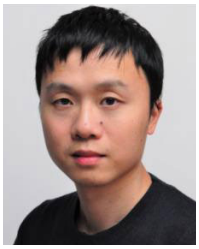

WEIJIA YUAN (Senior Member, IEEE) received the bachelor's degree from Tsinghua University, in 2006, and the Ph.D. degree from the University of Cambridge, in 2010. He was a Research Associate with the Engineering Department, University of Cambridge, and a Junior Research Fellow with the Wolfson College, University of Cambridge, from 2010 to 2011. He joined the University of Bath, as a Lecturer/Assistant Professor, in 2011, where he was later promoted to a Reader/Associate Professor, in 2016. He joined the University of Strathclyde, as a Professor, in 2018. He is currently leading a research team of more than ten members in the area applied superconductivity including energy storage, fault current limiters, machines and power transmission lines. His work also involves renewable energy integration and power system stability using energy storage systems.